International Journal of Minerals, Metallurgy and Materials
Volume 26, Number 3, March 2019, Page 337
https://doi.org/10.1007/s12613-019-1742-8

Hot-corrosion behavior of Cr_2O_3–CNT-coated ASTM-SA213-T22 steel in a molten salt environment at 700°C

Khushdeep Goyal[1)], *Hazoor Singh*[2)], *and Rakesh Bhatia*[2)]

1) Department of Mechanical Engineering, Punjabi University, Patiala-147002, India
2) Mechanical Engineering Section, Yadavindra College of Engineering, Talwandi Sabo, India
(Received: 6 June 2018; revised: 21 August 2018; accepted: 29 August 2018)

Abstract: The present work investigates the hot-corrosion behavior of carbon nanotube (CNT)-reinforced chromium oxide coatings on boiler steel in a molten salt (Na_2SO_4–60wt%V_2O_5) environment at 700°C under cyclic conditions. The coatings were deposited via the high-velocity oxygen fuel process. The uncoated and coated steel samples were subjected to hot corrosion in a silicon tube furnace at 700°C for 50 cycles. The kinetics of the corrosion behavior was analyzed through mass-gain measurements after each cycle. The corrosion products were analyzed by X-ray diffraction, scanning electron microscopy, and energy-dispersive X-ray analysis techniques. The results revealed that uncoated steel suffered spallation of scale because of the formation of nonprotective Fe_2O_3 scale. The coated steel samples exhibited lower mass gains with better adhesiveness of oxide scale with the steel alloy until the end of exposure. The CNT-reinforced coatings were concluded to provide better corrosion resistance in the hot-corrosion environment because of the uniform dispersion of CNTs in the coating matrix and the formation of protective chromium oxides in the scale.

Keywords: carbon nanotubes; corrosion; thermal spray; porosity; composite; boiler steel

1. Introduction

The development of new high-temperature materials is important for increasing the power output of coal-fired thermal power plants [1–3]. These new materials include thermal spray coatings, which are used on boiler steels to reduce hot corrosion at high temperatures [4–6]. The use of low-grade fuels, along with the presence of high temperatures and contaminants such as sodium, sulfur, and vanadium, leads to hot corrosion of boiler components. The hot corrosion degrades the properties of the boiler steels, ultimately leading to premature failure of boiler components [4,7–8]. Thermal spray coatings can increase the lifespan of boiler components used in high-temperature environments [9–10]. When powder spraying techniques are used to deposit these coatings, the resultant coatings are porous, with large numbers of pores. The corrosive elements attack the substrate steels through these pores and thereby induce corrosion [11–12]. This attack leads to the formation of an oxide layer on the surface of the substrate steel. Sidhu *et al.* [13] have reported that the formation of such an oxide layer is the main cause of failure of these coatings in high-temperature environments.

Some researchers have attempted to improve the corrosion resistance of such coatings by altering their microstructure by varying the parameters used in the spraying technique or by applying post treatments to already developed coatings [14–17]. Li *et al.* [18] have enhanced the surface flatness and corrosion resistance of coatings by laser heating. A few authors have altered the microstructure by mixing conventional powders with ceramic powders, cermets, and rare-earth oxides. Rani *et al.* [19] added Cr_2O_3 to Al_2O_3 powder to enhance the hot-corrosion resistance by the formation of protective oxides of Cr and Al. Saremi *et al.* [20] decreased the thickness of the oxide layer by depositing a composite coating of alumina in an yttria-stabilized zirconia matrix, resulting in enhanced high-temperature corrosion resistance. Yugeswaran *et al.* [21] reported that composite coatings contain more interfaces than conventional coatings, which causes blockage of pores. This blocking hinders the

Corresponding author: Khushdeep Goyal E-mail: khushgoyal@yahoo.com

diffusion of corroding species and improves the corrosion resistance of these coatings.

After the discovery of carbon nanotubes (CNTs) by Iijima [22], many researchers have reported that, because of their exceptional mechanical properties, CNTs offer substantial opportunities for developing new composite materials [23–25]. Deng *et al.* [26] used CNTs to fabricate aluminum-based composites and revealed that the CNTs acted as bridges across voids and cracks and were uniformly dispersed in the aluminum matrix. The uniform dispersion of CNTs in an aluminum matrix also led to improvements in mechanical properties [27–28]. Kim *et al.* [29] enhanced the wear resistance of composites by reinforcing them with 1wt% CNTs. Feng *et al.* [30] revealed that CNTs can be used to enhance the microstructural properties of composites by entering and filling the pores. A few researchers have developed CNT-reinforced Al_2O_3 thermal spray coatings with enhanced room temperature corrosion and wear resistance [31–35]. However, the literature contains no previous studies of the high-temperature corrosion behavior of CNT-reinforced Cr_2O_3 coatings on boiler-tube steels.

The present work focuses on the hot-corrosion behavior of high-velocity oxygen fuel (HVOF)-sprayed chromium oxide and 1wt%, 2wt%, 4wt%, 6wt%, and 8wt% CNT–Cr_2O_3 composite coatings on ASTM-SA213-T22 (T22) boiler-tube steel at 700°C in a molten salt environment. The T22 boiler-tube steel was selected as the substrate material in this work because it is used in the boiler components in Indian thermal power plants. Na_2SO_4–60wt%V_2O_5 salt is used because it simulates the conditions of molten sulfates and vanadates deposits, which are formed when combustion products of low-grade fuels condense in actual boilers. Mass-gain measurements during each cycle were used to investigate the kinetics of hot corrosion, and the corrosion products were characterized by X-ray diffraction (XRD), scanning electron microscopy with energy-dispersive analysis (SEM/EDAX), and X-ray mapping techniques.

2. Experimental

2.1. Preparation of coatings

The base material (T22) in the form of a boiler-tube was procured from Guru Nanak Dev Thermal Power Plant, Bathinda, India; samples with dimensions of 22 mm × 15 mm × 3 mm were cut from the boiler-tube. Commercially available chromium(III) oxide (Cr_2O_3) powder with particle sizes of (45 ± 10) μm was mixed with CNT powder in a ball mill. Five different composite powders were prepared with various contents of CNTs: 1wt% CNTs, 2wt% CNTs, 4wt% CNTs, 6wt% CNTs, and 8wt% CNTs. The Cr_2O_3 powder and composite powders were sprayed onto the T22 samples at Metallizing Equipment Company Pvt. Ltd., Jodhpur, India, using their high velocity oxy fuel (HVOF, HIPOJET-2100) equipment. A total of six different coatings were developed on the T22 samples (Table 1). The thickness of the coatings was monitored with a Minitest-2000 thin-film thickness gauge during the spraying process; the thickness of all of the coatings was in the range from 250 to 255 μm. The porosity of all of the coatings was evaluated from SEM micrographs of cross-sections via the image analysis method using the LEICA Image analyzer software. The porosity of the Cr_2O_3 coating was 1.90%. With the addition of CNTs to the Cr_2O_3, the porosity of the composite coatings decreased. The porosity values of the coatings with 1wt%, 2wt%, 4wt%, 6wt%, and 8wt% CNTs were found to be 1.84%, 1.79%, 1.71%, 1.61%, and 1.52%, respectively. The literature related to fabrication and investigation of the properties of these coatings has been published elsewhere by same authors [36–38].

Table 1. Composition of different coatings wt%

Type of coating	Cr_2O_3	CNTs
Cr_2O_3	100	0
Cr_2O_3–1wt%CNT	99	1
Cr_2O_3–2wt%CNT	98	2
Cr_2O_3–4wt%CNT	96	4
Cr_2O_3–6wt%CNT	94	6
Cr_2O_3–8wt%CNT	92	8

2.2. Hot-corrosion studies in molten salt (Na_2SO_4–60wt%V_2O_5)

Hot-corrosion experiments were carried out in a silicon tube furnace at 700°C. The physical dimensions (length, breadth, and thickness) of the samples were measured before the experiment. Acetone was used to rinse the samples before they were dried in hot air to remove moisture from their surface. The samples were then preheated to 250°C in an oven, and a salt mixture of Na_2SO_4–60wt%V_2O_5 dissolved in distilled water was coated onto the samples with a camel-hair brush. The loading of salt on the samples was kept in the range from 3.0 to 5.0 mg·cm^{-2} [39]. The samples were placed in alumina boats and then dried in an oven for 3 h at 100°C; they were subsequently weighed along with the alumina boats. The samples and alumina boats were then subjected to hot corrosion in a silicon tube furnace at 700°C for 50 cycles. Each cycle consisted of 1 h of exposure in the furnace followed by 20 min of cooling at room temperature [19,39]. After each cycle, the mass of the sample along with its alumina boat was recorded. After the

hot-corrosion experiments, the corroded samples were analyzed by XRD, SEM/EDAX, and cross-sectional tests to characterize the corrosion products.

3. Results

3.1. Visual examination

The macrographs of the uncoated T22 samples and the samples coated with Cr_2O_3 reinforced with different contents of CNTs, as obtained after hot corrosion in the molten salt environment (Na_2SO_4–60wt%V_2O_5) at 700°C for 50 cycles, are shown in Fig. 1. For the uncoated T22 steel (Fig. 1(a)), scale formation was observed at the end of the second cycle at 700°C; swelling of the scale was observed at the end of 18th cycle during the experiment. Minor spalling with cracks began appearing during the 23rd cycle, and the scale formation continued until the 50th cycle. In the case of the Cr_2O_3-coated T22, as shown in Fig. 1(b), the color of the sample turned greenish-black after the 8th cycle and minor cracks appeared in the coating after the 45th cycle. The macrographs of the CNT-reinforced Cr_2O_3-coated T22 steel samples are shown in Figs. 1(c)–1(g). All of the CNT-reinforced coatings were found to be intact, smooth, and without any signs of cracks or spallation.

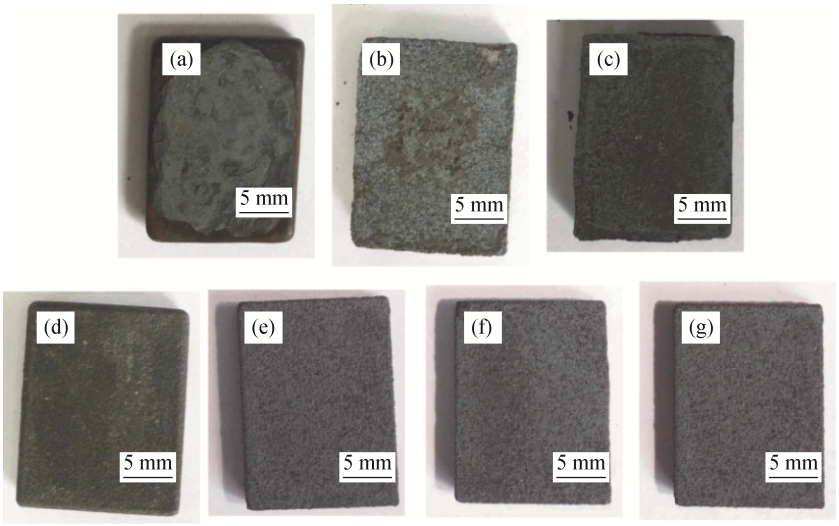

Fig. 1. Macrographs of the corroded uncoated and coated T22 samples after hot corrosion at 700°C: (a) uncoated; (b) Cr_2O_3; (c) Cr_2O_3–1wt%CNT; (d) Cr_2O_3–2wt%CNT; (e) Cr_2O_3–4wt%CNT; (f) Cr_2O_3–6wt%CNT; (g) Cr_2O_3–8wt%CNT.

3.2. Mass-change kinetics

The mass-change plots for all of the samples after hot corrosion are shown in Fig. 2. Mass-gain measurements were used to identify the kinetics of corrosion, where a large mass-change indicates a high corrosion rate. In the case of hot corrosion of uncoated T22 steel at 700°C, the mass gain (mass gain indicates the mass gain per unit area) was slow for first 5 cycles but increased after 5th cycle and continued to increase until the end of 50 cycles. The plot shows that the mass gain of Cr_2O_3-coated T22 steel increased after the 20th cycle; however, the mass-gain rate was much lower than that of the uncoated T22 sample. The mass-gain rate decreased when CNTs were introduced into the Cr_2O_3 coating matrix, as evident in the plots shown in Fig. 2.

The cumulative mass gain for the Cr_2O_3-coated T22 steel was 4.20 mg·cm^{-2}, which is substantially less than that for uncoated T22 steel (76.94 mg·cm^{-2}). The Cr_2O_3 coating reduced the overall mass gain by 94.5%. With the addition of CNTs to the Cr_2O_3 coating, the overall mass gain further decreased after hot corrosion at 700°C for 50 cycles. The cumulative mass gain for the Cr_2O_3–1wt%CNT-, Cr_2O_3–2wt%CNT-, Cr_2O_3–4wt%CNT-, Cr_2O_3–6wt%CNT-, and Cr_2O_3–8wt%CNT-coated T22 steel after hot corrosion at 700°C for 50 cycles was found to be 3.27, 2.38 mg·cm^{-2}, 1.89, 1.82, and 1.18 mg·cm^{-2}, respectively. Therefore, the Cr_2O_3–1wt%CNT, Cr_2O_3–2wt%CNT, Cr_2O_3–4wt%CNT, Cr_2O_3–6wt%CNT, and Cr_2O_3–8wt%CNT coatings on T22 steel reduced the cumulative mass gain of the T22 steel by 94.8%, 96.9%, 97.5%, 97.6%, and 98.5%, respectively. After hot corrosion in a molten salt environment at 700°C for 50 cycles, the Cr_2O_3–8wt%CNT coating on T22 steel exhibited the highest corrosion resistance among the investigated coatings.

A plot of (mass gain)^2 versus the number of cycles is shown in Fig. 3; it shows the nature of the fit for high-temperature corrosion at 700°C for uncoated and coated T22 samples. The curve for uncoated T22 steel shows some deviation from a parabolic rate law, whereas the samples coated with Cr_2O_3 and CNT-reinforced Cr_2O_3

very nearly follow a parabolic rate law. The parabolic rate constant (K_p) was calculated from the slope of the fitted linear regression line. The K_p values, along with the cumulative mass gain after exposure, are shown in Table 2. The K_p values for the coated T22 samples were found to be substantially lower than that for the uncoated T22 steel sample. The cumulative mass gain was found to decrease with increasing CNT content in the Cr_2O_3 coating matrix.

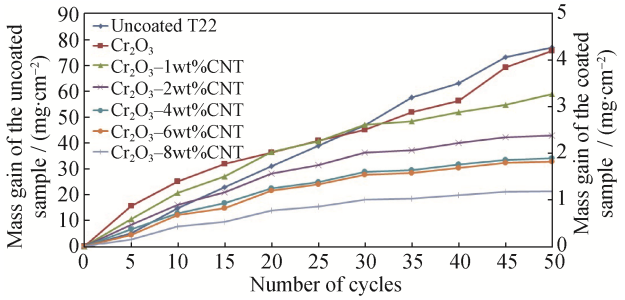

Fig. 2. Mass gain versus time (number of cycles) for all samples after hot corrosion.

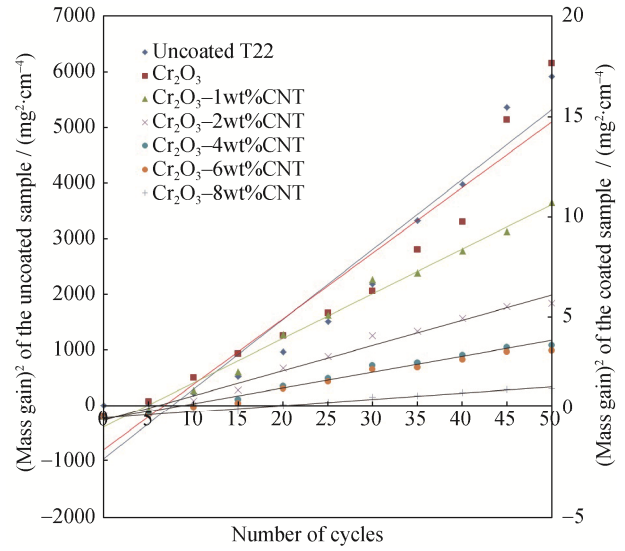

Fig. 3. Plot of (mass gain)^2 versus the number of cycles (50 cycles) for all samples after hot corrosion.

Table 2. Parabolic rate constants and cumulative mass gains for all samples

Type of coating	K_p / (10^{-10} g^2·cm^{-4}·s^{-1})	Cumulative mass gain / (mg·cm^{-2})
Uncoated T22	328.87	76.94
Cr_2O_3	0.98	4.20
Cr_2O_3–1wt%CNT	0.59	3.27
Cr_2O_3–2wt%CNT	0.31	2.38
Cr_2O_3–4wt%CNT	0.20	1.89
Cr_2O_3–6wt%CNT	0.18	1.82
Cr_2O_3–8wt%CNT	0.08	1.18

3.3. XRD analysis

The XRD analysis results for the uncoated samples and the CNT-reinforced coatings after hot corrosion at 700°C are shown in Figs. 4(a)–4(g). In the case of the corroded sample of uncoated T22, Fe oxides are identified in the scale (Fig. 4(a)). XRD analyses of the Cr_2O_3 and CNT-reinforced Cr_2O_3 coatings after corrosion indicate Cr_2O_3 as the main phase. Peaks of carbon are observed in the XRD patterns of all of the CNT-reinforced-Cr_2O_3-coated T22 steel samples (Figs. 4(c)–4(g)). Minor peaks of Na_2SO_4 and V_2O_5 are also evident in the XRD patterns of all of the samples.

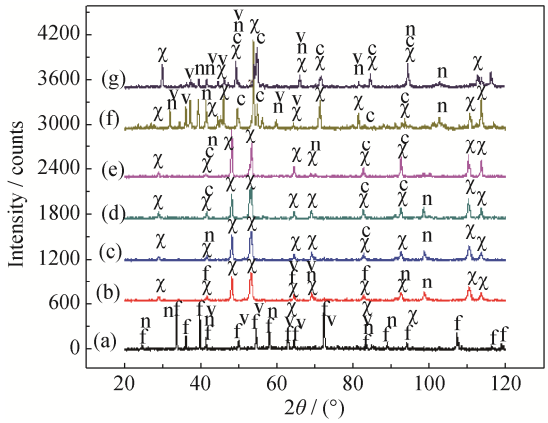

Fig. 4. XRD patterns of corroded uncoated and coated T22 samples after hot corrosion at 700°C: (a) uncoated; (b) Cr_2O_3; (c) Cr_2O_3–1wt%CNT; (d) Cr_2O_3–2wt%CNT; (e) Cr_2O_3–4wt%CNT; (f) Cr_2O_3–6wt%CNT; (g) Cr_2O_3–8wt%CNT. f—Fe_2O_3; c—Carbon; n—Na_2SO_4; v—V_2O_5; χ—Cr_2O_3.

3.4. SEM/EDAX analyses

FE-SEM micrographs of uncoated and coated T22 steel after hot corrosion in a Na_2SO_4–60wt%V_2O_5 environment at 700°C are given in Fig. 5, along with the corresponding EDAX analysis results. The oxide scale of corroded uncoated T22 (Fig. 5(a)) appears to comprise randomly oriented flakes with irregular shapes and also appears to be porous. The EDAX analysis results show that the oxide scale mainly consists of iron and oxygen, which indicates the possible formation of iron(III) oxide (Fe_2O_3). The scale composition also indicates the presence of minor amounts of Na and V. The micrograph of Cr_2O_3-coated T22 after hot corrosion at 700°C is shown in Fig. 5(b) and indicates a nodular structure with white and gray contrast phases. EDAX analysis at points 1 and 2 revealed that the scale mainly consists of Cr and O. The presence of Fe, Na, and V is indicated at point 1, and that of Fe and V is indicated at point 2. The presence of Fe might be due to diffusion from the substrate to the oxide scale during hot corrosion. The micro-

graph of the Cr_2O_3–1wt%CNT-coated T22 steel (Fig. 5(c)) indicates a substantial amount of Cr and O with small amounts of C, Na, and V in the scale. The indication of C confirms the presence of CNTs in the oxide scale. The micrographs and EDAX analysis results for the Cr_2O_3–2wt%CNT-, Cr_2O_3–4wt%CNT-, Cr_2O_3–6wt%CNT-, and Cr_2O_3–8wt%CNT-coated T22 boiler steel are shown in Figs. 5(d)–5(g), respectively. The scales of all of the samples appear to be uniform and intact, with a regular morphology. The EDAX analysis indicated that the scale was primarily composed of Cr and O, with a substantial presence of C. The amount of C increased with increasing CNT content in the Cr_2O_3 coating. The minor presence of Na and V is also evident in the EDAX analysis results for each selected point after hot corrosion at 700°C. These results confirm the presence of molten salt elements.

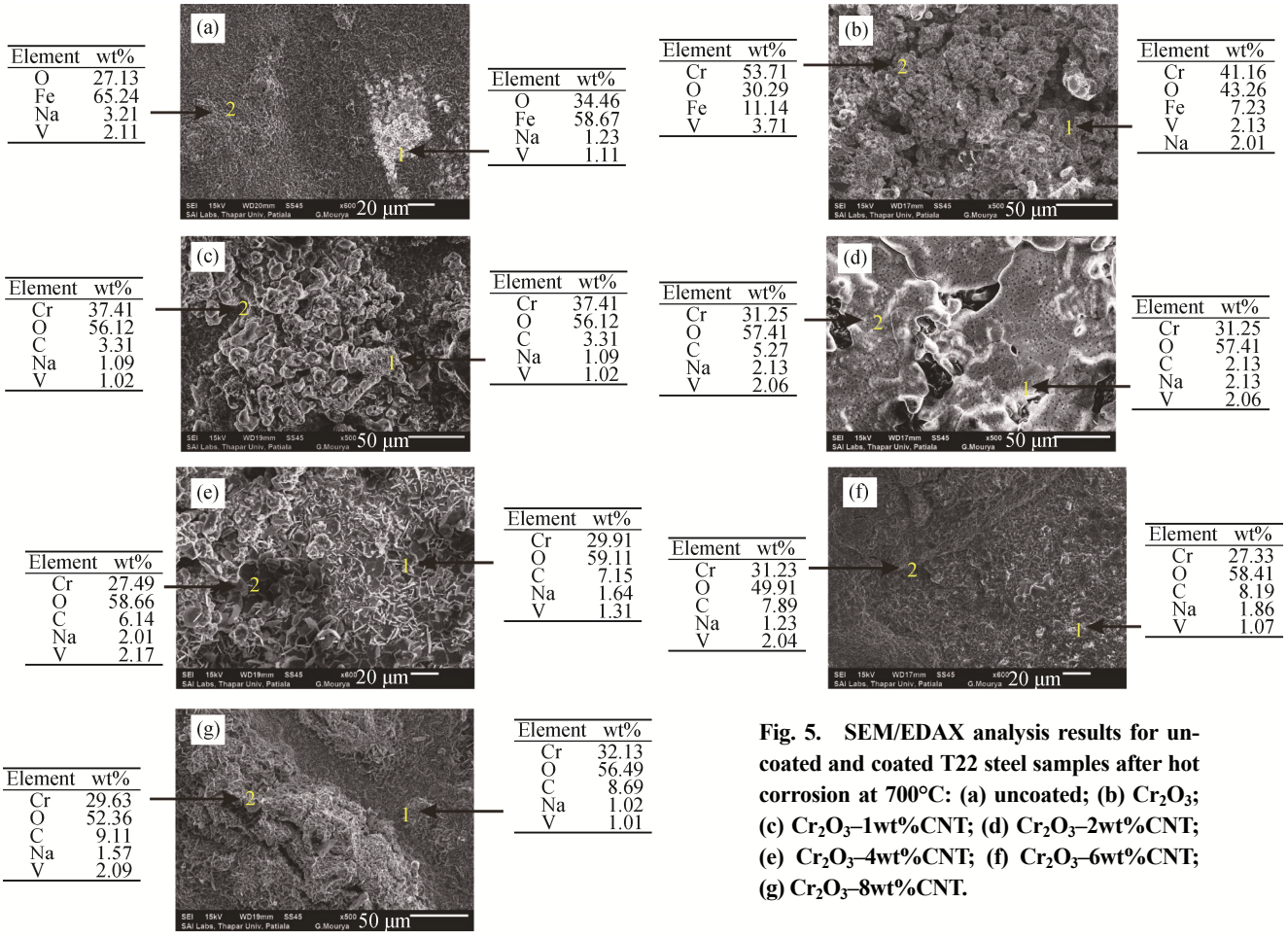

Fig. 5. SEM/EDAX analysis results for uncoated and coated T22 steel samples after hot corrosion at 700°C: (a) uncoated; (b) Cr_2O_3; (c) Cr_2O_3–1wt%CNT; (d) Cr_2O_3–2wt%CNT; (e) Cr_2O_3–4wt%CNT; (f) Cr_2O_3–6wt%CNT; (g) Cr_2O_3–8wt%CNT.

4. Discussion

CNT-reinforced-Cr_2O_3-matrix-based composite coatings were deposited onto T22 steel with various CNT contents. The thickness of all types of coatings was found to be in the range from 250 to 255 µm. The porosity of the conventional Cr_2O_3 coating was 1.90%, which was further reduced with increasing CNT content in the Cr_2O_3 matrix. Keshri and Agarwal [40] have attributed this decrease in porosity to the absorption of more heat by powder particles due to the dispersed CNTs, which has led to the enhanced melting of powder particles.

The hot corrosion of T22 steel in a Na_2SO_4–60wt%V_2O_5 environment at 700°C for 50 cycles resulted in the formation of thick, porous, and a nonprotective Fe_2O_3 scale. During the hot-corrosion studies, the corrosion rate of uncoated samples increase at a comparatively higher rate during the initial cycles, possibly because of the formation of cracks in the oxide scale. The cracks appeared on the surface of the sample after the initial cycles during the experiment. The value of the parabolic rate constant was 328.87×10^{-10} $g^2 \cdot cm^{-4} \cdot s^{-1}$, and the total mass gain after 50 cycles was 76.94 $mg \cdot cm^{-2}$. This high mass gain and the formation of nonprotective Fe_2O_3 during hot-corrosion experiments in a molten salt environment has also been reported by Rani *et al.* [19] and Goyal *et al.* [39], and was also confirmed by XRD

analysis and by SEM/EDAX analysis at selected points. The cross-sectional EDAX analysis also showed that Fe and O were present in the oxide scale, confirming the formation of Fe_2O_3.

The Cr_2O_3 coating on T22 steel mitigated the mass gain of the steel by 94.5% after hot corrosion at 700°C. Minor cracks and spallation of scale were observed during exposure to hot corrosion. Better corrosion resistance of the T22 steel was provided by the protective Cr_2O_3 coating, whose formation was also confirmed by XRD analysis. Butler *et al.* [41] and Sadeghimeresht *et al.* [42] reported that the Cr_2O_3 phase is thermodynamically stable to very high temperatures because of its high melting point. The minor spallation of the sample during hot corrosion studies was due to the formation of nonprotective Fe_2O_3 as a minor phase in the scale. The formation of Fe_2O_3 might be attributable to the penetration of Fe through the voids and cracks in the coating. The SEM micrographs indicated a nodular structure with gray and white contrast phases, which might be due to the oxides of chromium and iron in the scale. EDAX and cross-sectional analyses confirmed the presence of Cr, Fe, and O at selected points. The presence of Na and V might be due to the molten salt used in the experiments.

The mass-gain plots indicated that protection from hot corrosion at 700°C in a molten salt environment was provided by the CNT-reinforced-Cr_2O_3 coatings on T22 steel. All of the CNT–Cr_2O_3 coatings were intact, without cracks or spallation, after 50 cycles. The Cr_2O_3–1wt%CNT, Cr_2O_3–2wt%CNT, Cr_2O_3–4wt%CNT, Cr_2O_3–6wt%CNT, and Cr_2O_3–8wt%CNT coatings on T22 steel reduced the cumulative mass gain of the T22 steel by 94.8%, 96.9%, 97.5%, 97.6%, and 98.5%, respectively. The Cr_2O_3–8wt%CNT-coated T22 sample exhibited the highest corrosion resistance among the investigated coatings exposed to a molten salt environment at 700°C for 50 cycles. Smaller mass-gain values for the Cr_2O_3–CNT-coated T22 steel samples may be due to the presence of CNTs in the Cr_2O_3 matrix. The XRD analysis indicated that the main phase was Cr_2O_3, accompanied by carbon, which confirmed the presence of CNTs in the coating matrix even after hot-corrosion studies. Singhal *et al.* [43] and Ahmad *et al.* [44] have also reported XRD peaks of carbon in the coating matrix. The comparatively better corrosion resistance of the CNT-reinforced coatings might be due to the presence of CNTs and the formation of a protective Cr_2O_3 layer in the scale during hot-corrosion exposure at 700°C. The CNT-reinforced coatings were found to be intact, as revealed by SEM micrographs, and EDAX analysis further confirmed the presence of Cr, O, and C at selected points. The cross-sectional analysis further confirmed the uniform distribution of carbon throughout the coating cross-section. The uniform presence of CNTs was responsible for the decrease in porosity of the coatings, which further helped to prevent attack of the corroding species at the T22 steel substrate during the hot-corrosion experiments in a molten salt environment. In the literature, CNTs have been reported to be able to enter the voids in such coatings to reduce their porosity [33,45], and a dense coating always provides better corrosion protection than a porous coating. Therefore, the reinforcement of CNTs in the Cr_2O_3 matrix enhanced the corrosion resistance of the conventional Cr_2O_3 coating.

5. Conclusions

In this research work, the hot-corrosion behavior of CNT-reinforced Cr_2O_3 coatings on T22 steel was investigated at 700°C in a molten salt environment. The uncoated T22 steel exhibited greater mass gain and a higher corrosion rate, resulting in the formation of thick, porous, and nonprotective Fe_2O_3 scale during hot-corrosion studies in a molten salt environment at 700°C. The mass gain of the Cr_2O_3-coated T22 steel was 94.5% lower than that of the uncoated steel because of the formation of protective oxides of chromium. Some cracks with minor spallation of scale were observed after hot-corrosion studies because of the formation of iron oxide. The Fe_2O_3 was formed by the penetration of Fe through the voids in the Cr_2O_3 coating. All of the Cr_2O_3–CNT coatings showed comparatively lower mass gains than the Cr_2O_3 coating, and the mass gain decreased with increasing CNT content in the coating. All of the Cr_2O_3–CNT coatings were intact, with no cracks or spallation, after 50 cycles during the hot-corrosion experiments. The Cr_2O_3–1wt%CNT, Cr_2O_3–2wt%CNT, Cr_2O_3–4wt%CNT, Cr_2O_3–6wt%CNT, and Cr_2O_3–8wt%CNT coatings on T22 steel reduced the cumulative mass gain of the T22 steel by 94.8%, 96.9%, 97.5%, 97.6%, and 98.5%, respectively. The XRD analysis of all of the CNT-reinforced coatings indicated that Cr_2O_3 and carbon phases were present; the presence of Cr, O, and C was also confirmed by EDAX and cross-sectional analyses. The addition of CNTs resulted in a reduction in porosity by the CNTs filling the voids in the Cr_2O_3 coating, with interlocking of particles; the interlocked CNTs blocked the penetration of corroding species, thereby enhancing the corrosion resistance of the composite coatings.

References

[1] C.A. Duarte, E. Espejo, and J.C. Martinez, Failure analysis of

the wall tubes of a water-tube boiler, *Eng. Fail. Anal.,* 79(2017), p. 704.

[2] F.F. Alia, T. Kurniawan, Y.P. Asmara, M.H.B. Ani, and A.B.D. Nandiyanto, High temperature oxidation in boiler environment of chromized steel, *IOP Conf. Ser.: Mater. Sci. Eng.*, 257(2017), art. No. 012086.

[3] D. Kumar, K.N. Pandey, and D.K. Das, Microstructure studies of air-plasma-spray-deposited CoNiCrAlY coatings before and after thermal cyclic loading for high-temperature application, *Int. J. Miner. Metall. Mater.*, 23(2016), No. 8, p. 934.

[4] Q. Ding, X.F. Tang, and Z.G. Yang, Failure analysis on abnormal corrosion of economizer tubes in a waste heat boiler, *Eng. Fail. Anal.*, 73(2017), No. 1, p. 129.

[5] A. Keyvani and M. Bahamirian, Oxidation resistance of Al_2O_3-nanostructured/CSZ composite compared to conventional CSZ and YSZ thermal barrier coatings, *Mater. Res. Express*, 3(2016), No. 10, p. 105047.

[6] T. Dudziak, A. Olbrycht, A. Polkowska, L. Boron, P. Skiersk i, A. Wypych, A. Ambroziak, and A. Krezel, High temperature coatings from post processing Fe-based chips and Ni-based alloys as a solution for critical raw materials, *IOP Conf. Ser.: Mater. Sci. Eng.*, 329(2018), art. No. 012010.

[7] M. Loghman-Estarki, R.S. Razavi, H. Edris, S.R. Bakhshi, M. Nejati, and H. Jamali, Comparison of hot corrosion behavior of nanostructured ScYSZ and YSZ thermal barrier coatings, *Ceram. Int.*, 42(2016), No. 6, p. 7432.

[8] R. Aadhavan, S. Bhanuchandar, and K.S. Babu, Surface coating of ceria nanostructures for high-temperature oxidation protection, *Mater. Res. Express*, 5(2018), No. 4, p. 045025.

[9] K. Goyal, H. Singh, and R. Bhatia, Current status of thermal spray coatings for high temperature corrosion resistance of boiler steel, *J. Mater. Metall. Eng.*, 6(2016), No. 1, p. 29.

[10] C.P. Jiang, Y.Z. Xing, F.Y. Zhang, and J.M. Hao, Microstructure and corrosion resistance of Fe/Mo composite amorphous coatings prepared by air plasma spraying, *Int. J. Miner. Metall. Mater.*, 19(2012), No. 7, p. 657.

[11] S. Saladi, J. Menghani, and S. Prakash, Hot corrosion behaviour of detonation-gun sprayed Cr_3C_2–NiCr coating on inconel-718 in molten salt environment at 900°C, *Trans. Ind. Inst. Met.*, 67(2014), No. 5, p. 623.

[12] L.I. Huang, H.M. Meng, L.K. Liang, S. Li, and J.H. Shi, Effects of heat treatment on the corrosion resistance of carbon steel coated with $LaMgAl_{11}O_{19}$ thermal barrier coatings, *Int. J. Miner. Metall. Mater.*, 22(2015), No. 10, p. 1050.

[13] V.P.S. Sidhu, K. Goyal, and R. Goyal, Comparative study of corrosion behaviour of HVOF-coated boiler steel in actual boiler environment of a thermal power plant, *J. Aust. Ceram. Soc.*, 53(2017), No. 2, p. 925.

[14] P. Bengtsson and T. Johannesson, Characterization of microstructural defects in plasma-sprayed thermal barrier coatings, *J. Therm. Spray Technol.*, 4(1995), No. 3, p. 245.

[15] G. Fargas, D. Casellas, L. Llanes, and M. Anglada, Thermal shock resistance of yttria-stabilized zirconia with Palmqvist indentation cracks, *J. Eur. Ceram. Soc.*, 23(2003), No. 1, p. 107.

[16] S. Mohsen, A. Abbas, and K. Akira, Bond coat oxidation and hot corrosion behaviour of plasma sprayed YSZ coating on Ni superalloy, *Trans. JWRI*, 36(2007), No. 1, p. 41.

[17] T.S. Dong, X.K. Zhou, G.L. Li, L. Liu, and R. Wang, Microstructure and corrosive wear resistance of plasma sprayed Ni-based coatings after TIG remelting, *Mater. Res. Express*, 5(2018), No. 2, art. No. 026411.

[18] B. Li, Y. Jin, J.H. Yao, Z.H. Li, Q.L. Zhang, and X. Zhang, Influence of laser irradiation on deposition characteristics of cold sprayed Stellite-6 coatings, *Opt. Laser Technol.*, 100(2018), p. 27.

[19] A. Rani, N. Bala, and C.M. Gupta, Characterization and hot corrosion behavior of D-gun sprayed Cr_2O_3–75% Al_2O_3 coated ASTM-SA210-A1 boiler steel in molten salt environment, *Anti-Corros. Methods Mater.*, 64(2017), No. 5, p. 515.

[20] M. Saremi, A. Afrasiabi, and A. Kobayashi, Microstructural analysis of YSZ and YSZ/Al_2O_3 plasma sprayed thermal barrier coatings after high temperature oxidation, *Surf. Coat. Tehcnol.*, 202(2008), No. 14, p. 3233.

[21] S. Yugeswaran, C.P. Yoganand, A. Kobayashi, K. Paraskevopoulos, and B. Subramanian, Mechanical properties, electrochemical corrosion and in-vitro bioactivity of yttria stabilized zirconia reinforced hydroxyapatite coatings prepared by gas tunnel type plasma spraying, *J. Mech. Behav. Biomed. Mater.*, 9(2012), p. 22.

[22] S. Iijima, Helical microtubules of graphitic carbon, *Nature*, 354(1991), No. 6348, p. 56.

[23] E.T. Thostenson, C.Y. Li, and T.W. Chou, Nanocomposites in context, *Compos. Sci. Technol.*, 65(2005), No. 3-4, p. 491.

[24] K.T. Lau, M. Chipara, H.Y. Ling, and D. Hui, On the effective elastic moduli of carbon nanotubes for nanocomposite structures, *Composites Part B*, 35(2004), No. 2, p. 95.

[25] M. Bocanegra-Bernal, C. Dominguez-Rios, J. Echeberria, A. Reyes-Rojas, A. Garcia-Reyes, and A. Aguilar-Elguezabal, Effect of low-content of carbon nanotubes on the fracture toughness and hardness of carbon nanotube reinforced alumina prepared by sinter, HIP and sinter + HIP routes, *Mater. Res. Express*, 4(2017), No. 8, art. No. 085004.

[26] C.F. Deng, D.Z. Wang, X.X. Zhang, and A.B. Li, Processing and properties of carbon nanotubes reinforced aluminum composites, *Mater. Sci. Eng. A*, 444(2007), No. 1-2, p. 138.

[27] A.M.K. Esawi, K. Morsi, A. Sayed, M. Taher, and S. Lanka, Effect of carbon nanotube (CNT) content on the mechanical properties of CNT-reinforced aluminium composites, *Compos. Sci. Technol.*, 70(2010), No. 16, p. 2237.

[28] M. Sharma and V. Sharma, Chemical, mechanical, and thermal expansion properties of a carbon nanotube-reinforced aluminum nanocomposite, *Int. J. Miner. Metall. Mater.*, 23(2016), No. 2, p. 222.

[29] I.Y. Kim, J.H. Lee, G.S. Lee, S.H. Baik, Y.J. Kim, and Y.Z. Lee, Friction and wear characteristics of the carbon nanotube–aluminum composites with different manufacturing conditions, *Wear*, 267(2009), No. 1-4, p. 593.

[30] Y. Feng, H.L. Yuan, and M. Zhang, Fabrication and properties of silver-matrix composites reinforced by carbon nanotubes, *Mater. Charact.*, 55(2005), No. 3, p. 211.

[31] A.K. Keshri, V. Singh, J. Huang, S. Seal, W. Choi, and A. Agarwal, Intermediate temperature tribological behavior of carbon nanotube reinforced plasma sprayed aluminum oxide coating, *Surf. Coat. Technol.*, 204(2010), No. 11, p. 1847.

[32] K. Balani, S.P. Harimkar, A. Keshri, Y. Chen, N.B. Dahotre, and A. Agarwal, Multiscale wear of plasma-sprayed carbon-nanotube-reinforced aluminum oxide nanocomposite coating, *Acta Mater.*, 56(2008), No. 20, p. 5984.

[33] C.F. Gutierrez-Gonzalez, A. Smirnov, A. Centeno, A. Fernández, B. Alonso, V.G. Rocha, R. Torrecillas, A. Zurutuza, and J.F. Bartolome, Wear behavior of graphene/alumina composite, *Ceram. Int.*, 41(2015), No. 6, p. 7434.

[34] W. Guo and H.Y. Tam, Effects of carbon nanotubes on wear of WC/Co micropunches, *Int. J. Adv. Manuf. Technol.*, 72(2014), No. 1-4, p. 269.

[35] E.Edward Anand and S. Natarajan, Effect of carbon nanotubes on corrosion and tribological properties of pulse-electrodeposited Co–W composite coatings, *J. Mater. Eng. Perform.*, 24(2015), No. 1, p. 128.

[36] K. Goyal, H. Singh, and R. Bhatia, Mechanical and microstructural properties of carbon nanotubes reinforced chromium oxide coated boiler steel, *World J. Eng.*, 15(2018), No. 4, p. 429.

[37] K. Goyal, H. Singh, and R. Bhatia, Experimental investigations of carbon nanotubes reinforcement on properties of ceramic-based composite coating, *J. Aust. Ceram. Soc.*, 3(2018), No. 7, p. 1.

[38] K. Goyal, H. Singh, and R. Bhatia, Effect of carbon nanotubes on properties of ceramics based composite coatings, *Adv. Eng. Forum*, 26(2018), p. 53.

[39] A. Goyal, R. Singh, and G. Singh, Study of high-temperature corrosion behavior of D-gun spray coatings on ASTM-SA213, T-11 steel in molten salt environment, *Mater. Today Proc.*, 4(2017), No. 2, p. 142.

[40] A.K. Keshri and A. Agarwal, Splat morphology of plasma sprayed aluminum oxide reinforced with carbon nanotubes: A comparison between experiments and simulation, *Surf. Coat. Technol.*, 206(2011), No. 2-3, p. 338.

[41] T.M. Butler, J.P. Alfano, R.L. Martens, and M.L. Weaver, High-temperature oxidation behavior of Al–Co–Cr–Ni–(Fe or Si) multicomponent high-entropy alloys, *JOM*, 67(2015), No. 1, p. 246.

[42] E. Sadeghimeresht, N. Markocsan, T. Hussain, M. Huhtakangas, and S.V. Joshi, Effect of SiO_2 dispersion on chlorine-induced high temperature corrosion of HVAF-sprayed NiCrMo coating, *Corrosion*, 74(2018), No. 9, p. 984.

[43] S.K. Singhal, R. Pasricha, M. Jangra, R. Chahal, S. Teotia, and R.B. Mathur, Carbon nanotubes: Amino functionalization and its application in the fabrication of Al-matrix composites, *Powder Technol.*, 215-216(2012), p. 254.

[44] I. Ahmad, M. Unwin, H. Cao, H. Chen, H. Zhao, A. Kennedy, and Y.Q. Zhu, Multi-walled carbon nanotubes reinforced Al_2O_3 nanocomposites: Mechanical properties and interfacial investigations, *Compos. Sci. Technol.*, 70(2010), No. 8, p. 1199.

[45] G.Q. Han, Z.H. Wang, K. Liu, S.B. Li, X. Du, and W.B. Du, Synthesis of CNT-reinforced AZ31 magnesium alloy composites with uniformly distributed CNTs, *Mater. Sci. Eng. A*, 628(2015), No. 1, p. 350.